NÖHÜ Müh. Bilim. Derg. / NOHU J. Eng. Sci., 2025; 14(2), 532-541

Niğde Ömer Halisdemir Üniversitesi Mühendislik Bilimleri Dergisi
Niğde Ömer Halisdemir University Journal of Engineering Sciences

Araştırma makalesi / Research article

www.dergipark.org.tr/tr/pub/ngumuh / www.dergipark.org.tr/en/pub/ngumuh

Transforming ladle furnace slag into an efficient catalyst for hydrogen production by ammonia decomposition

Pota ocağı cürufunun amonyak ayrışması yoluyla hidrojen üretimi için verimli bir katalizöre dönüştürülmesi

Samira F. Kurtoğlu Öztulum[1,*]

[1]*Department of Chemical and Biological Engineering, Koç University, Rumelifeneri Yolu, Sariyer, 34450 Istanbul, Türkiye*
[1] *Koç University TÜPRAŞ Energy Center (KUTEM), Koç University, Rumelifeneri Yolu, Sariyer, 34450 Istanbul, Türkiye*
[1] *Department of Materials Science and Technology, Faculty of Science, Turkish-German University, Sahinkaya Cad., Beykoz, 34820 Istanbul, Türkiye*

Abstract

Ladle furnace slag (LFS), a byproduct of steel production, was modified via HCl treatment and calcination to obtain an efficient catalyst for ammonia decomposition. The unmodified catalyst (LFS-C500) and its modified counterpart (MLFS-C500) were thoroughly characterized by a combination of techniques, including temperature programmed reduction (TPR), X-ray diffraction (XRD), scanning electron microscopy coupled with energy dispersive X-ray spectroscopy (SEM/EDX), and X-ray fluorescence (XRF). MLFS-C500 outperformed LFS-C500, achieving 96.3% ammonia conversion at 700 °C and a space velocity of 6 000 ml NH_3/(h × g_{cat}), with a lower activation energy (131.7 kJ/mol) compared to LFS-C500 (153.0 kJ/mol). The superior performance of MLFS-C500 is attributed to its higher iron content, which successfully forms Fe crystallites upon reduction in H_2, and its enhanced surface structure, resulting from the removal of calcium compounds upon HCl modification. This work demonstrates how an industrial waste can be effectively valorised into low-cost catalysts for CO_x-free hydrogen production.

Keywords: Ammonia decomposition, Hydrogen storage, Heterogeneous catalysis, Ladle furnace slag, Catalyst characterization

Öz

Pota ocağı cürufu (LFS), çelik üretiminin bir yan ürünü olup, HCl ile muamele ve kalsinasyon yoluyla amonyak ayrışması için verimli bir katalizör haline getirilmiştir. Tepkimeden önce ve sonra modifiye edilmemiş katalizör (LFS-C500) ve modifiye edilmiş katalizör (MLFS-C500), sıcaklık programlı indirgeme (TPR), X-ışını kırınımı (XRD), enerji dağılımlı X-ışını spektroskopisi ile taramalı elektron mikroskobu (SEM/EDX) ve X-ışını floresansı (XRF) gibi tekniklerle ayrıntılı bir şekilde karakterize edilmiştir. MLFS-C500, 700 °C'de ve 6000 ml NH_3/(h × g_{kat}) boşluk hızında %96.3 amonyak dönüşümü sağlayarak, LFS-C500'den daha üstün bir performans sergilemiştir. Ayrıca, MLFS-C500 (131.7 kJ/mol), LFS-C500'e (153.0 kJ/mol) kıyasla daha düşük bir aktivasyon enerjisi göstermiştir. MLFS-C500'ün üstün performansı, modifikasyon ile kalsiyum içeren bileşiklerin giderilmesi sonucu artan demir içeriği ve bu demir içeriğinin başarılı bir şekilde H_2 ile indirgeme sırasında Fe kristalitlerine dönüştürülmesi ile gelişmiş yüzey yapısına atfedilmiştir. Bu çalışma, endüstriyel atıkların CO_x açığa çıkarmadan hidrojen üretimi için düşük maliyetli katalizörlere nasıl etkin bir şekilde dönüştürülebileceğini göstermektedir.

Anahtar Kelimeler: Amonyak ayrışması, Hidrojen depolama, Heterojen kataliz, Pota ocağı cürufu, Katalizör karakterizasyonu

1 Introduction

Hydrogen is a clean energy carrier with a high energy-to-weight ratio providing an energy density of 120 MJ/kg [1]. However, the low density of hydrogen creates challenges for its safe and efficient storage, which must be resolved for hydrogen to become a viable replacement for fossil fuels.

One method for storing hydrogen involves using high-pressure tanks, however this approach suffers from high gas pressures, creating safety risks [2]. Another option is the liquefaction of hydrogen, though it is energy-intensive and costly [2]. Hydrogen can be lost because of boil-off, making this method less practical. Physisorption of hydrogen on porous materials like zeolites [3], metal organic frameworks [4], or carbon-based materials is another approach, but the low adsorption capacity and need for low temperatures limits its practical application. Alternatively, storing hydrogen chemically in molecules such as methane, methanol, or ammonia [5] can overcome these issues. Among these molecules, ammonia stands out thanks to its carbon-free composition, high volumetric and gravimetric hydrogen density, existing infrastructure, and non-flammability, making it an ideal choice for CO_x-free hydrogen storage [6].

High-performance catalysts are essential for cracking ammonia to hydrogen and nitrogen. Ru-, Ni-, Co-, and Fe-based catalysts have shown promise, with Ru-based catalysts leading in performance [7]. However, the high cost and scarcity of Ru are major drawbacks. Although Fe-, Co- and Ni-based catalysts are cheaper alternatives, complex production routes or the need for expensive support materials

* Sorumlu yazar / Corresponding author, e-posta / e-mail: samira.kurtoglu@tau.edu.tr (S. F. Kurtoğlu Öztulum)
Geliş / Received: 21.10.2024 Kabul / Accepted: 12.02.2025 Yayımlanma / Published: 15.04.2025
doi: 10.28948/ngumuh.1571359

can hinder their use, as well. Thus, there is a strong need for an affordable and efficient catalyst synthesized using simple methods for hydrogen production from ammonia.

One alternative potential solution is to create cost-effective catalysts by reusing industrial wastes through simple modifications. For example, fly ash, a byproduct of coal combustion rich in SiO_2, Al_2O_3, and Fe_2O_3, could be modified through heat treatment and acid washing to serve as a support material for Ru in ammonia decomposition [8]. This modification enhanced the surface area of fly ash, improving Ru dispersion and enhancing ammonia decomposition rates. In another study, Cao and colleagues modified red mud, a byproduct of the aluminum production rich in Fe_2O_3, and used it as a support for Ni [9]. Modified red mud-supported Ni catalyst with a Ni loading of 12 wt% showed the highest activity for ammonia decomposition. These studies highlight the potential of utilizing waste materials as catalyst supports to produce cost-effective catalysts. Additionally, these waste materials can be used directly as bulk catalysts upon simple modifications and without the addition of external metals, offering an even more economical approach. For example, Kurtoğlu et al. demonstrated that red mud could be transformed into an Fe-based catalyst upon simple acid and heat treatments [10, 11]. The intrinsic Fe content of red mud acted as the active site, and the produced red mud-derived iron-based catalysts provided record high hydrogen production rates for ammonia decomposition compared to other non-noble metal-based catalysts reported in the literature.

Motivated from these promising findings, this study aims to transform ladle furnace slag (LFS), a byproduct of steel industry, into a catalyst for ammonia decomposition without the addition of external metals. LFS is one of the four major slags produced in the iron and steel industry, alongside blast furnace slag, basic oxygen furnace slag, and electric arc furnace slag [12]. LFS is produced in the final steps of steel production and is classified as a basic slag. It is rich in CaO, MgO (which also contributes to its basicity), Al_2O_3, SiO_2, and Fe_2O_3 [13].

In this work, LFS was modified by an acid digestion-precipitation method, commonly applied to industrial wastes such as red mud to enhance surface area and reduce alkali content [14]. Both the as-received LFS and modified ladle furnace slag (MLFS) were tested for ammonia decomposition to produce CO_x-free hydrogen. This study is the first demonstration of ladle furnace slag being used as a catalyst in ammonia decomposition. This approach demonstrates how industrial wastes can be transformed into efficient and cost-effective catalysts, offering a sustainable solution for hydrogen production while addressing waste management in the steel industry.

2 Materials and methods

2.1 Sample preparation

LFS used in this study was kindly provided by Kardemir-Karabük Demir Çelik Sanayi ve Ticaret A.Ş. LFS was calcined at 500 °C in static air for 2 hours following a ramp rate of 5 °C/min to obtain LFS-C500. MLFS was obtained by following the route described elsewhere [14]. In short, 25 gram LFS was first mixed with 100 ml distilled water and then mixed with 150 ml of 6 M HCl solution. This mixture was digested in a Milestone Microwave Digestion System (SK-10) with a temperature controller, operating at 350 W at 220 °C. The resulting sample was precipitated by adding aqueous ammonia until a pH of 8 was reached. The resulting sample was washed several times with distilled water, separated by centrifugation, and dried in a vacuum oven overnight at 110 °C. The resulting sample was coded as MLFS. When MLFS was calcined at 500 °C in static air for 2 hours following a ramp rate of 5 °C/min, MLFS-C500 was obtained.

2.2 Characterization

X-ray diffraction (XRD) measurements were carried out using a Rigaku MiniFlex 600 equipped with Cu Kα radiation (40 kV, 15 mA). A Zeiss Ultra Plus field emission scanning electron microscope operating at ultra vacuum and at an accelerating voltage of 5 kV was used to obtain scanning electron microcopy (SEM) images. Energy-dispersive X-ray spectroscopy (EDX) imaging was performed on this microscope with a XFlash 5010 detector. X-ray fluorescence (XRF) measurement was performed on the as-received LFS using a Panalytical/Axios MAX spectrometer, by preparing a pellet of approximately 10 g of sample. Temperature programmed reduction (TPR), CO_2 desorption (CO_2-TPD), and NH_3 desorption (NH_3-TPD) was conducted on a Micromeritics AutoChem II 2920. For TPR, 100 mg sample was placed in a U-shaped quartz reactor. The sample was reduced in 15 ml/min pure H_2 flow at 700 °C for 2 hours, following a ramp rate of 5 °C/min. During H_2-reduction, the effluent gas was analyzed by a thermal conductivity detector (TCD). For CO_2-TPD, 0.1 g of sample was initially treated under helium flow at 300 °C for 1 hour, after which the sample was allowed to cool to room temperature. Subsequently, CO_2 was introduced at room temperature for 1 hour to enable adsorption. The temperature was then ramped up to 600 °C at a rate of 10 °C/min under helium flow. For both NH_3- and CO_2-TPD experiments, the effluent gas was analyzed by using a TCD. Brunauer–Emmett–Teller (BET) surface area analysis was conducted using an Anton Paar Nova800 Physisorption Analyzer. For this purpose, 0.8 g of sample was used for LFS and LFS-C500, while 0.2 g was utilized for MLFS and MLFS-C500. Prior to analysis, all samples were degassed under vacuum at 120 °C for 8 hours.

2.3 Catalytic activity measurement

300 mg of catalyst was sandwiched between two quartz wool layers to fix the catalyst bed in the middle of a quartz reactor. The quartz reactor with the catalyst was placed in a Carbolite split-tube furnace. Reduction in H_2 was performed prior to catalytic performance measurement at the same conditions used for TPR measurements (at 700 °C for 2 hours, ramp rate = 5 °C/min). After reduction while at 700 °C, argon was used to purge the catalyst bed at a flow of 50 ml/min for 15 min. Then, the gas was changed to NH_3 at a flow of 50 ml/min (using 300 mg catalyst, this corresponds to a space velocity of 10 000 ml $NH_3/(h \times g_{cat})$) at the same temperature of 700 °C to start the activation period that

lasted for approximately 13 hours. Once the induction period was complete, the temperature was decreased to obtain the Arrhenius plots and to measure the activation energy of the catalysts (below an ammonia conversion of 25%). At constant space velocity of 10 000 ml $NH_3/(h \times g_{cat})$, the temperature was varied between 550 and 650 °C to obtain the Arrhenius plot of LFS-C500 and between 500 and 600 °C for MLFS-C500. Subsequently, the temperature was increased back to 700 °C and the space velocity was adjusted to 3000, 6000, 20 000, 30 000, and 40 000 ml $NH_3/(h \times g_{cat})$ to further investigate the potential of the catalysts. To ensure data stability, at least 45 minutes were allowed for each data point. Thus, each experiment lasted approximately 21 hours (after the H_2 reduction): 13 hours for the induction period, 4 hours for obtaining the Arrhenius plot, and the final 4 hours for investigating the space velocity. Conversion was monitored continuously by a Hidden QGA mass spectrometer that was calibrated for H_2, N_2, and NH_3 using the corresponding *m/z* ratios of 2, 28, and 17.

3 Results and discussion

The XRF analysis result of the as-received LFS is provided in Table 1. Components such as SiO_2, MgO, and Al_2O_3, commonly used as support materials in catalysis, are prominent in the LFS. Additionally, oxides such as K_2O, Na_2O, MnO, or BaO that can act as promoters, are also present among the detected components of LFS. Fe_2O_3 is notable for providing active sites for ammonia decomposition reaction.

Table 1. Composition of LFS obtained by XRF.

Compound	Concentration (wt%)
CaO	51.15
SiO_2	20.05
MgO	9.13
Al_2O_3	8.92
SO_3	3.77
Fe_2O_3	3.50
F	1.35
Na_2O	0.53
MnO	0.49
TiO_2	0.31
Others	0.79

Figure 1 presents the SEM images captured with a backscattered electron detector, with corresponding EDX spectra of as-received LFS and its modified counterpart (MLFS). Table 2 shows the elemental composition of LFS and MLFS obtained by analysis of the EDX spectrum provided in Figure 1b and d. Consistent with the XRF results of LFS (Table 1), the EDX spectrum confirms that the most abundant component in LFS is Ca, indicated by the most intense peak in its spectrum (Figure 1b, Table 2). After modification, however, the Ca content decreased significantly (Figure 1d, Table 2), making MLFS a more suitable catalyst because of the increased relative concentrations of the oxides of Fe, Si, Al and Mg, combined with the reduction in Ca. Particularly, the increase in Fe content from 2.74 wt% to 7.93% upon modification is important, as Fe sites will act as active sites for the ammonia decomposition reaction.

Additionally, Figure 1d and Table 2 reveal a significant increase in the Cl content of MLFS, a residual byproduct left from the acid modification process. Therefore, to eliminate the Cl-containing compounds, both LFS and MLFS were calcined at 500 °C in air prior to further use in catalytic performance tests, as Cl is a known poison in catalysis [15]. Previous studies have demonstrated that a calcination at 500 °C effectively removes Cl-containing residues from materials modified by similar processes [14].

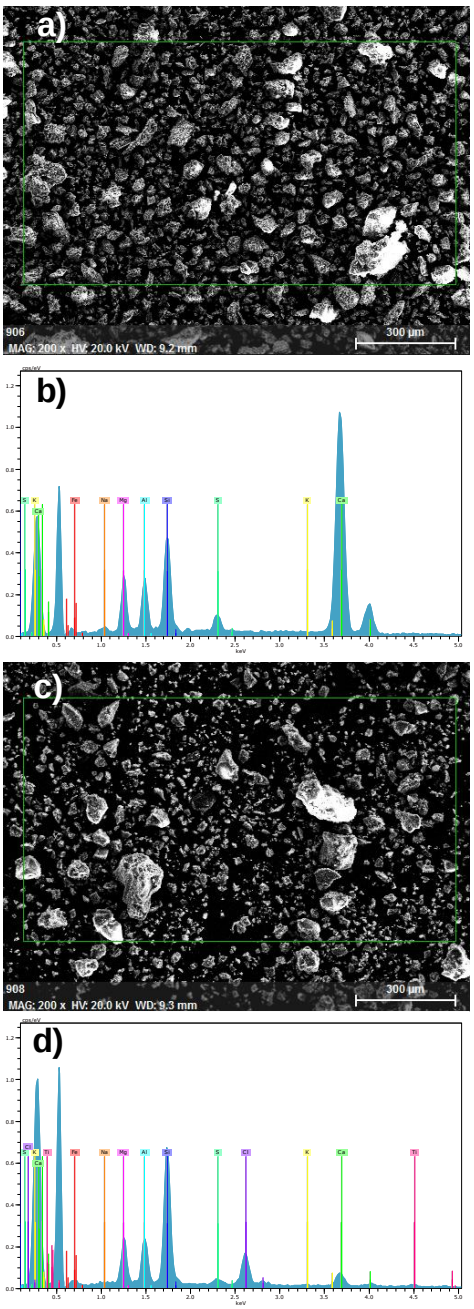

Figure 1. SEM image of a) LFS and b) corresponding EDX spectrum, SEM image of c) MLFS and d) corresponding EDX spectrum.

Table 2. Elemental composition of LFS and MLFS obtained by EDX spectrum analysis.

Chemical	Composition (%)	
	LFS	MLFS
Ca	62.65	8.79
Si	12.96	35.57
Al	8.05	12.90
K	0.55	1.15
Mg	8.74	11.62
S	2.96	3.69
Fe	2.74	7.93
Na	1.36	1.08
Cl	-	15.15
Ti	-	2.14

Figure 2 shows the XRD patterns of LFS, MLFS, LFS-C500 and MLFS-C500. The XRD pattern of as-received LFS exhibits five major phases. Peaks at 15.7, 20.5, 21.8, 23.2, 26.2, 29.6, 32.4, 32.7, 35.6, 36.8, and 47.5° indicate the presence of colcio-olivine, a calcium silicate, which was observed in LFS also by Sundhararasu et al. [16]. Peaks at 29.8, 33.4, and 41.6° were attributed to grossular, a calcium-aluminum garnet [16]. Furthermore, periclase (MgO) was identified by peaks present at 42.8 and 62.2°, as also observed in another LFS sample by Aponte and colleagues [17]. Moreover, mayenite was detected by peaks located at 18.0, 29.8, 33.4, 41.2, and 46.9°, a phase commonly reported in previous LFS studies [13, 17, 18]. Moreover, calcite was observed as demonstrated by peaks labelled with "5" in Figure 2, in accordance with previous reports [16, 17]. These observed phases are consistent with the XRF results presented in Table 1.

Upon calcination of LFS, the crystal structure remained mostly unchanged, as observed in the XRD pattern of LFS-C500 (Figure 2, black line). However, the acid digestion (Figure 2, green line) causes a significant decrease in crystallinity, along with the disappearance of all phases observed in as-received LFS. Both MLFS and MLFS-C500 exhibit poor crystallinity, showing that upon acid digestion and reprecipitation, the resulting product is mostly in an amorphous phase. A similar decrease in crystallinity was also observed for another industrial waste, red mud, after being digested in acid [14]. The only prominent peak observed in the XRD of MLFS was at 26.5°, which may indicate the presence of quartz. However, the significant reduction in intensity of this peak following calcination (in MLFS-C500) decreases the likelihood of its attribution to quartz. Instead, it is more plausibly associated with a chlorine-containing byproduct formed during the acid modification process. This hypothesis is supported by previous studies [14], which reported the disappearance of similar peaks along with a concomitant reduction in chlorine content upon calcination.

To further investigate the structural changes in LFS upon modification, SEM images at higher magnifications were taken using a secondary electron detector (Figure 3). The SEM image of LFS (Figure 3a) reveals distinct morphologies, confirming its heterogeneous structure, as also confirmed by XRD analysis of LFS. The needle-like structures observed in Figure 3a are attributed to the presence of calcite, as they resemble previously reported needle-fibre calcite [19]. Upon acid modification (Figure 3b), these needle-like structures are no longer visible, supporting this observation. Additionally, it is worth noting that after modification and calcination (MLFS-C500), the morphology retains a porous structure, even after high-temperature calcination, with several pores appearing on the surface of MLFS-C500 (Figure 3c).

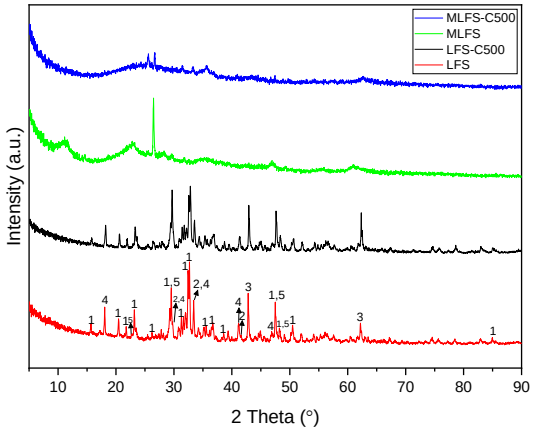

Figure 2. XRD patterns of LFS, MLFS, LFS-C500 and MLFS-C500. 1–Calcioolivine (γ-Ca_2SiO_4), 2–Grossular ($Ca_3Al_2(SiO_4)_3$), 3–Periclase (MgO), 4–Mayenite ($Ca_{12}Al_{14}O_{33}$), 5–Calcite ($CaCO_3$).

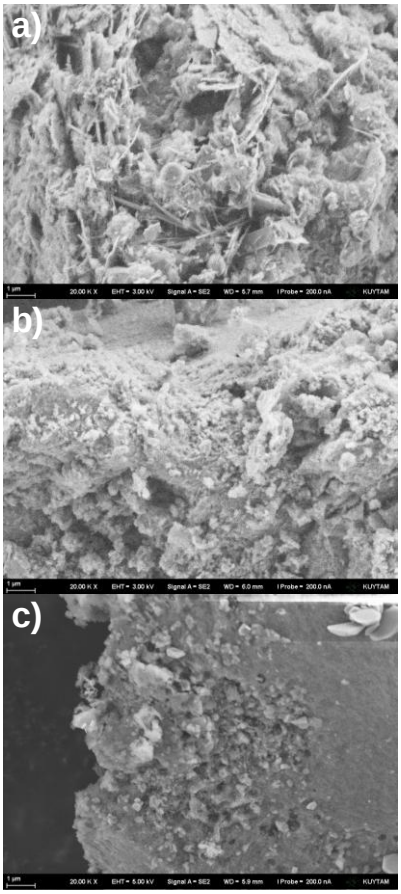

Figure 3. SEM images obtained on a) LFS, b) MLFS, and c) MLFS-C500 at a magnification of 20 000×.

Surface area, pore volume, and pore sizes of the samples are provided in Table 3. The data show that the modification process significantly increased the surface area of LFS from 1.2 to 184.9 m^2/g (MLFS), highlighting the effectiveness of the modification procedure. A subsequent calcination step, performed on MLFS to remove residual impurities from acid digestion, reduced the surface area to 139.9 m^2/g. Despite this decrease, the surface area remained substantially higher compared to the as-received LFS. In contrast, simple calcination performed directly on LFS (LFS-C500) had minimal impact on surface area, as shown by the low value of 1.5 m^2/g for MLFS-C500. Comparing the pore volumes, it is evident that MLFS and MLFS-C500 exhibit a remarkable increase (approximately two orders of magnitude) compared to LFS and LFS-C500.

Table 3. Textural properties of LFS, LFS-C500, MLFS, and MLFS-C500.

Sample	BET surface area (m^2/g)	Pore volume (cm^3/g)	Pore size (nm)
LFS	1.2	0.0036	4.0
LFS-C500	1.5	0.0051	4.0
MLFS	184.9	0.2926	3.7
MLFS-C500	139.9	0.3787	7.1

To evaluate the acid and base surface properties of a representative sample (MLFS-C500), NH_3-TPD and CO_2-TPD measurements were performed, respectively. The CO_2-TPD analysis revealed three main desorption peaks located at 142, 425, and 513 °C (Figure 4a). The peak at 142 °C corresponds to weak basic sites, while the peaks at 425 and 513 °C, though less intense, clearly indicate the presence of strong basic sites. These findings suggest that MLFS-C500 possesses a variety of basic sites capable of donating electrons to active sites, potentially playing a significant role in ammonia decomposition. This is particularly relevant because the rate-limiting step in ammonia decomposition, the combinative desorption of nitrogen from the surface, is known to be accelerated by basic supports. In contrast, the NH_3-TPD profile of MLFS-C500 exhibits a single peak at 117 °C, most likely corresponding to physisorbed NH_3 (Figure 4b). While a few very low-intensity shoulders and features are present, they are indistinct and therefore not labeled on the graph. This indicates that MLFS-C500 predominantly provides basic rather than acidic sites, making it a promising candidate for utilization in NH_3 decomposition.

Prior to NH_3 decomposition reaction, catalysts must be reduced under H_2 to convert the iron oxide content present in LFS-C500 and MLFS-C500 to the active bulk Fe phase. To confirm the conversion of Fe_2O_3 to Fe during this reduction, TPR measurements were conducted (Figure 5). The most intense peak at 630 °C in the TPR curve of LFS-C500 (Figure 5a) is attributed to the reduction of Ca-containing phases, because it was reported earlier that CaO provides reduction peaks at around 610 °C [20]. The overlapping peaks at approximately 407 and 442 °C might be related to the first reduction step of Fe_2O_3, indicating the reduction of Fe_2O_3 to Fe_3O_4. The reduction of Fe_2O_3 to Fe_3O_4 was reported at 380 °C for pure Fe_2O_3 [21] and at 442 °C in a Fe_2O_3-rich waste material [10] under identical ramp rates during TPR to those used in this study. The shoulder appearing at 670 °C might be associated with the further reduction of Fe_3O_4 to FeO and FeO to Fe, as these transitions are typically reported as a broad peak occurring between 400 and 600 °C [10, 21]. However, it should be noted that these less intense peaks at 407, 442, and 670 °C can be also associated with the localized reduction of calcium-containing compounds particularly at grain boundaries or defect sites.

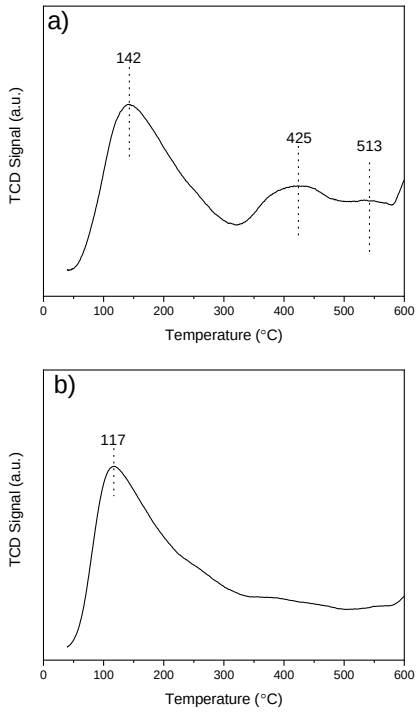

Figure 4. a) CO_2-TPD and b) NH_3-TPD profiles of MLFS-C500.

The TPR curve of MLFS-C500 is shown in Figure 5b. The peak associated with the Ca-containing compounds' reduction, which was observed at 630 °C in LFS-C500 (Figure 5a), became broader and shifted to a lower temperature (550 °C) after modification. This is expected because of the decrease in calcium content, as evidenced by EDX analysis. The peak at 550 °C appears to be a combined peak, representing the reduction of the left Ca-containing compounds, as well as the second step of Fe_2O_3 reduction (Fe_3O_4 to FeO and FeO to Fe). Moreover, the shoulder appearing at 453 °C might be associated with the first step of Fe_2O_3 reduction (Fe_2O_3 to Fe_3O_4).

The TPR curves of both LFS-C500 and MLFS-C500 confirm that the selected reduction temperature, ramp rate, and duration were appropriate for successfully reducing the species present in the samples, as the TCD signals stabilized for both catalysts after approximately 150 minutes of time-on-stream (Figure 5a and b).

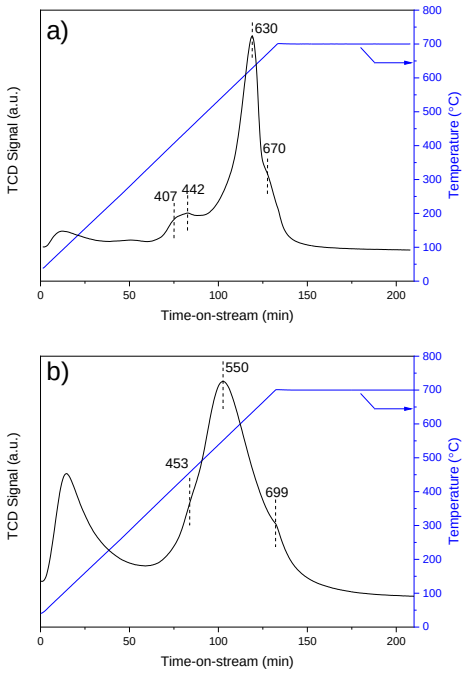

Figure 5. TPR curves of a) LFS-C500 and b) MLFS-C500.

The reduced versions of LFS-C500 and MLFS-C500 were further characterized using SEM (Figure 6). The SEM image of LFS-C500 reduced in H_2 (Figure 6a) clearly shows the relatively flat morphology with some granular structures. In contrast, even upon a reduction at 700 °C, the porous morphology on MLFS-C500 is still retained (Figure 6b), resembling the SEM image of its fresh counterpart (Figure 3c).

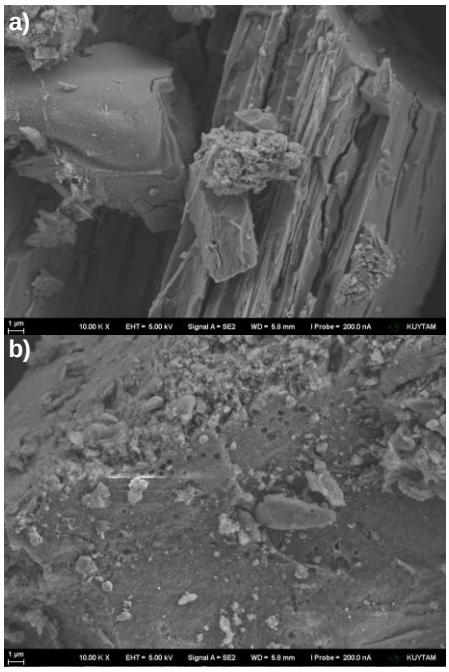

Figure 6. SEM images obtained on the reduced LFS-C500 and b) reduced MLFS-C500 at a magnification of 10 000×.

XRD patterns obtained on the reduced catalysts are presented in Figure 7. While the reduced LFS-C500 did not show significant difference compared to the XRD pattern of fresh LFS-C500 (Figure 2, black line), the reduction of MLFS-C500 was highly effective in reducing the iron content, as evidenced by the very sharp and intense Fe peaks detected at 44.6, 65.0, and 82.3° (Figure 7, blue line). The absence of intense and well-defined bulk Fe peaks in the reduced form of LFS-C500 supports the fact that the reduction peaks observed at 407, 442, and 670 °C may be associated with the reduction of calcium-containing compounds (Figure 5a).

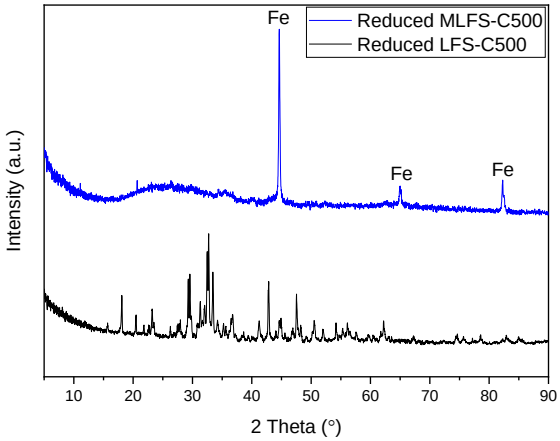

Figure 7. XRD patterns of reduced catalysts.

After confirming the successful reduction of components in both LFS-C500 and MLFS-C500 (Figure 5), the catalysts were tested for ammonia decomposition. The catalysts were first reduced in the catalytic testing system following the same procedure used for obtaining the TPR curves in Figure 5, after which the gas was switched to NH_3. Following the induction period at 700 °C (Figure 8a), the temperature was decreased to measure the activation energy (Figure 8b) of the catalysts, in the region where low conversions are reached (< 25 %).

As shown in Figure 8a, LFS-C500 completed its induction period within approximately 4 hours, while the ammonia conversion of MLFS-C500 steadily increased up to 13 hours time-on-stream. Although LFS-C500 achieved a stable ammonia conversion earlier, both catalysts were subjected to a 13-hour induction period prior to the activation energy measurements. At the end of this 13 h-induction period, LFS-C500 achieved an ammonia conversion of 53.3 % at a space velocity of 10 000 ml $NH_3/(h \times g_{cat})$ and at a temperature of 700 °C, whereas the modified counterpart (MLFS-C500) provided a significantly enhanced ammonia conversion of 80.1 % at identical conditions (Figure 8a).

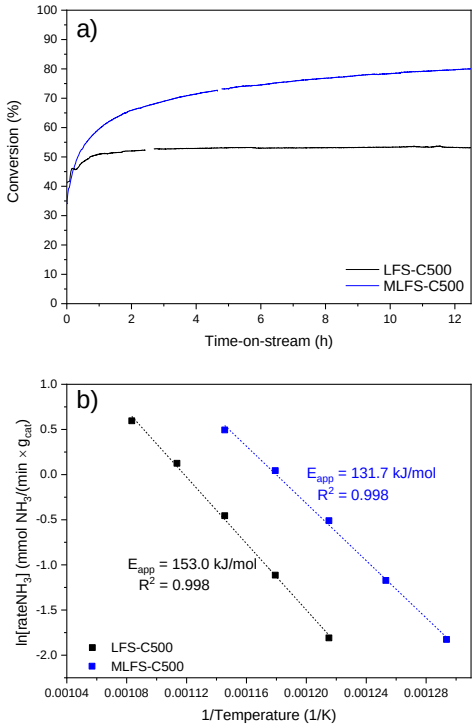

Figure 8. a) Activation period of the catalysts at 700 °C and at a space velocity of 10 000 ml NH_3/(h × g_{cat}) and b) Arrhenius plots of the catalysts.

The enhanced ammonia decomposition is further reflected by the catalysts' Arrhenius plots (Figure 8b). The activation energies of LFS-C500 and MLFS-C500 were determined as 153.0 and 131.7 kJ/mol, respectively, typical values for iron-based catalysts [22, 23, 24]. It should be noted that the modification not only increased the number of active sites by reducing the CaO content, but also resulted in a decrease in activation energy.

To further evaluate the catalytic performance of the two catalysts, the space velocity was varied at 700 °C and the ammonia conversions (Figure 9a) and corresponding H_2 production rates (Figure 9b) were obtained. As the space velocity decreases, fewer NH_3 molecules interact with each Fe active center, resulting in an increase in ammonia conversion, as shown in Figure 9a. However, while lower space velocity enhances ammonia conversion, the reduced NH_3 flow through the reactor leads to a decrease in hydrogen production rates per unit time, as illustrated in Figure 9b. The selection of the optimum space velocity depends on the specific requirements of the process. For applications prioritizing higher conversion rates and purer products, a space velocity of 3000 mL NH_3/(h × g_{cat}) seems more suitable. Conversely, in processes where unconverted NH_3 can be separated and higher hydrogen production rates are desired, higher space velocity values are more suitable. Hence, the optimum reaction conditions can be determined based on the specific needs of the application.

Data show that MLFS-C500 significantly outperformed LFS-C500, emphasizing the effectiveness of a simple acid modification followed by calcination for improving the structural characteristics and catalytic performance of slags. For instance, at a space velocity of 6 000 ml NH_3/(h × g_{cat}) and a temperature of 700 °C, MLFS-C500 provided an ammonia conversion of 96.3 % corresponding to a hydrogen production rate of 5.9 mmol H_2 / (min × g_{cat}). At identical conditions, LFS-C500 provided an ammonia conversion of 64.7 % and a hydrogen production rate of 4.0 mmol H_2 / (min × g_{cat}), markedly lower than its modified counterpart. Ammonia decomposition tests conducted at a large range of temperatures (Figure 9c) further demonstrate that MLFS-C500 outperforms LFS-C500 at all temperatures (Figure 8c). This enhanced performance is attributed to the increased iron content, resulting because of the decrease of the amount of CaO, the successful formation of iron crystallites, and the improved textural properties.

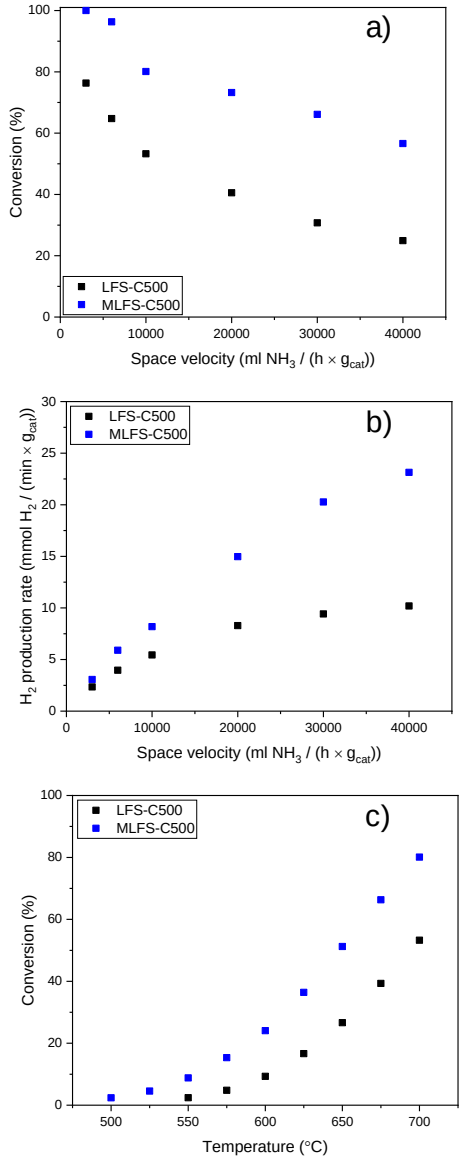

Figure 9. a) Ammonia conversions and b) H_2 production rates of the catalysts at varying space velocities at a constant temperature of 700 °C. c) Ammonia conversions at a constant space velocity of 10 000 ml NH_3/(h × g_{cat}) at varying temperatures.

The catalytic performance of the almost cost-free MLFS-C500 was compared with several non-noble metal-based ammonia decomposition catalysts reported in the literature (Table 4). For example, while a Fe-containing carbon nanotube catalyst provided 75.1 % conversion at a space velocity of 5 000 ml $NH_3/(h \times g_{cat})$, MLFS-C500 provided 96.3 % conversion at the same temperature at an even slightly higher space velocity of 6 000 ml $NH_3/(h \times g_{cat})$. Moreover, a Ni/SiO_2 catalyst provided 36.4 % conversion at 600 °C and at a space velocity of 30 000 ml $NH_3/(h \times g_{cat})$, while MLFS-C500 provided 24.1 % conversion at 10 000 ml $NH_3/(h \times g_{cat})$ at the same temperature. Furthermore, a two dimensional mica nanosheet-supported Fe catalyst provided 97.1 % conversion at 700 °C and at a space velocity of 30 000 ml $NH_3/(h \times g_{cat})$, while MLFS-C500 provided 66.1 % conversion at identical conditions. Although MLFS-C500 underperformed compared to some of these catalysts, it is important to highlight that MLFS-C500 is nearly cost-free and produced through simple techniques, whereas the Fe/mica nanosheet and Ni/SiO_2 catalysts are associated with higher costs.

Table 4. Catalytic performance comparison of MLFS-C500 with several non-noble metal-based catalysts in the literature.

Catalyst	Temperature (°C)	Conversion (%)	Space velocity ml $NH_3/(h \times g_{cat})$	Ref.
MLFS-C500	700	96.3	6 000	This study
MLFS-C500	700	73.3	20 000	This study
MLFS-C500	700	66.1	30 000	This study
MLFS-C500	600	24.1	10 000	This study
Fe- CNT	700	75.1	5 000	[25]
5%Fe/MS-HP	700	97.1	30 000	[23]
Co/CNTs	700	100	20 000	[25]
10% Ni/SiO_2	600	36.4	30 000	[26]

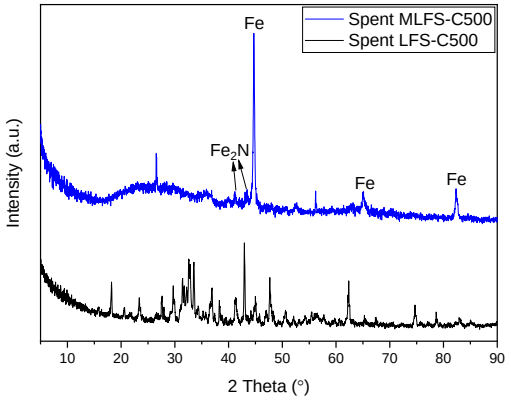

Figure 10. XRD patterns of spent catalysts.

XRD patterns of spent catalysts are presented in Figure 10. XRD pattern of spent MLFS-C500 shows iron crystallites, similar to its reduced form (Figure 7), pointing out that these iron crystallites are providing the active sites for this reaction. Low-intensity peaks belonging to Fe_2N were also observed, indicating the nitriding of a small amount of iron crystallites during the reaction. On the other hand, the spent catalyst of LFS-C500 shows no phase changes, resembling its fresh (Figure 2) and reduced (Figure 7) counterparts.

4 Conclusion

In this study, LFS, an industrial byproduct of steel production, was successfully transformed into an efficient catalyst for ammonia decomposition by a simple acid modification with HCl, followed by calcination at 500 °C. BET surface area measurements show that the surface area of as-received LFS significantly increased from 1.2 to 139.9 m^2/g upon acid modification and calcination, resulting in the modified slag, MLFS-C500. The TPR curves of both catalysts, LFS-C500 and MLFS-C500, confirmed the complete reduction of species in the slag-based catalysts when reduced in H_2 at 700 °C for 2 h following a ramp rate of 5 °C/min. XRD patterns of the reduced catalysts indicate that Fe crystallites are formed in MLFS-C500 upon reduction, while no significant phase changes were observed in LFS-C500. The successful formation of Fe crystallites in MLFS-C500 was attributed to its increased surface area resulting from modification. MLFS-C500 outperformed the unmodified LFS-C500 in ammonia decomposition tests, achieving higher ammonia conversion and hydrogen production rates. Specifically, MLFS-C500 provided 96.3 % ammonia conversion at a reaction temperature of 700 °C and a space velocity of 6 000 ml $NH_3/(h \times g_{cat})$. The activation energies of LFS-C500 and MLFS-C500 were determined to be 153.0 and 131.7 kJ/mol, respectively, demonstrating a decrease in activation energy upon modification. Furthermore, MLFS-C500 exhibited competitive performance compared to other non-noble metal-based catalysts, while offering the advantage of being nearly cost-free and produced through straightforward techniques. The enhanced catalytic performance of MLFS-C500 is attributed to its increased iron content, resulting from the removal of most of the calcium-containing compounds during modification, significantly improved surface area, and the formation of iron crystallites upon reduction which are the active sites for this reaction. This study highlights the potential of reusing industrial waste materials as low-cost catalysts for sustainable hydrogen production.

Acknowledgements

The author extends her sincere thanks to Prof. Alper Uzun from Koç University for his mentorship. Büşra Sekizkardeş is gratefully acknowledged for her help in modifying LFS. Special thanks to Dr. Barış Yağcı from Koç University Surface Science and Technology Center (KUYTAM) for his help in SEM/EDX measurements. The author thanks Ali Naci Zenginobuz for his support in BET surface area measurements. Koç University – Boron and Advanced Materials Applications and Research Center is gratefully

acknowledged for XRD measurements. Special thanks to Karabük Demir Çelik Sanayi ve Ticaret A.Ş. for kindly providing LFS.

Conflict of interest

The author declares no conflict of interest.

Similarity rate (iThenticate): 16 %

References

[1] M. R. Usman, Hydrogen storage methods: Review and current status. Renewable and Sustainable Energy Reviews, 167, 111743, 2022. https://doi.org/10.1016/j.rser.2022.112743.

[2] S. Ristig, M. Poschmann, J. Folke, O. Gómez-Cápiro, Z. Chen, N. Sanchez-Bastardo, R. Schlögl, S. Heumann, H. Ruland, Ammonia decomposition in the process chain for a renewable hydrogen supply. Chemie Ingenieur Technik, 94, 1413-1425, 2022. https://doi.org/10.1002/cite.202200003.

[3] J. Dong, X. Wang, H. Xu, Q. Zhao, J. Li, Hydrogen storage in several microporous zeolites. International Journal of Hydrogen Energy, 32, 4998-5004, 2007. https://doi.org/10.1016/j.ijhydene.2007.08.009.

[4] M. Hirscher and B. Panella, Hydrogen storage in metal–organic frameworks. Scripta Materialia, 56, 809-812, 2007. https://doi.org/10.1016/j.scriptamat.2007.01.005.

[5] W. I. F. David, Effective hydrogen storage: A strategic chemistry challenge. Faraday Discussions, 151, 399–414, 2011. https://doi.org/10.1039/C1FD00105A.

[6] S. Sun, Q. Jiang, D. Zhao, T. Cao, H. Sha, C. Zhang, H. Song, Z. Da, Ammonia as hydrogen carrier: Advances in ammonia decomposition catalysts for promising hydrogen production. Renewable and Sustainable Energy Reviews, 169, 112918, 2022. https://doi.org/10.1016/j.rser.2022.112918.

[7] J. E. Lee, J. Lee, H. Jeong, Y. K. Park, B. S. Kim, Catalytic ammonia decomposition to produce hydrogen: A mini-review. Chemical Engineering Journal, 475, 146108, 2023. https://doi.org/10.1016/j.cej.2023.146108.

[8] L. Li, S. Wang, Z. Zhu, X. Yao, Z. Yan, Catalytic decomposition of ammonia over fly ash supported Ru catalysts. Fuel Processing Technology, 89, 1106-1112, 2008. https://doi.org/10.1016/j.fuproc.2008.05.002.

[9] J. L. Cao, Z. L. Yan, Q. F. Deng, Y. Wang, Z. Y. Yuan, G. Sun, T. K. Jia, X. D. Wang, H. Bala, Z. Y. Zhang, Mesoporous modified-red-mud supported Ni catalysts for ammonia decomposition to hydrogen. International Journal of Hydrogen Energy, 39, 5747-5755, 2014. https://doi.org/10.1016/j.ijhydene.2014.01.169.

[10] S. F. Kurtoğlu, A. Uzun, Red Mud as an Efficient, Stable and Cost-Free Catalyst for CO_x-Free Hydrogen Production from Ammonia. Scientific Reports, 6, 32279, 2016. https://doi.org/10.1038/srep32279.

[11] S. F. Kurtoğlu, S. Soyer-Uzun, A. Uzun, Modifying the structure of red mud by simple treatments for high and stable performance in CO_x-free hydrogen production from ammonia. International Journal of Hydrogen Energy, 43, 20525-20537, 2018. https://doi.org/10.1016/j.ijhydene.2018.09.032.

[12] J. Setién, D. Hernández, J.J. González, Characterization of ladle furnace basic slag for use as a construction material. Construction and Building Materials, 23, 1788-1794, 2009. https://doi.org/10.1016/j.conbuildmat.2008.10.003.

[13] A Rađenović, J Malina, T Sofilić, Characterization of ladle furnace slag from carbon steel production as a potential adsorbent. Advances in Materials Science and Engineering, 1, 198240, 2013. https://doi.org/10.1155/2013/198240.

[14] S. F. Kurtoğlu, S. Soyer-Uzun, A. Uzun, Tuning structural characteristics of red mud by simple treatments. Ceramics International, 42, 17581-17593, 2020. https://doi.org/10.1016/j.ceramint.2016.08.072.

[15] W. Arabczyk, U. Narkiewicz, D. Moszyński, Chlorine as a poison of the fused iron catalyst for ammonia synthesis. Applied Catalysis A: General, 134, 331-338, 1996. https://doi.org/10.1016/0926-860X(95)00211-1.

[16] E. Sundhararasu, S. Tuomikoski, H. Runtti, T. Hu, T. Varila, T. Kangas, U. Lassi, Alkali-Activated Adsorbents from Slags: Column Adsorption and Regeneration Study for Nickel(II) Removal. Chemengineering, 5, 13, 2021. https://doi.org/10.3390/chemengineering5010013.

[17] D. Aponte, O. S. Martin, S. Valls del Barrio, M. Barra Bizinotto, Ladle Steel Slag in Activated Systems for Construction Use. Minerals, 10, 687, 2020. https://doi.org/10.3390/min10080687.

[18] Y. Wang, W. Ni, P. Suraneni, Use of Ladle Furnace Slag and Other Industrial By-Products to Encapsulate Chloride in Municipal Solid Waste Incineration Fly Ash. Materials, 12, 925, 2019. https://doi.org/10.3390/ma12060925.

[19] N. Durand, H. C. Monger, M. G. Canti, Calcium Carbonate Features. In: Interpretation of micromorphological features of soils and regoliths, Elsevier, pp. 149-194, 2010. https://doi.org/10.1016/B978-0-444-53156-8.00009-X.

[20] S. Sivasangar, M. S. Mastuli, A. Islam, Y. H. Taufiq-Yap, Screening of modified CaO-based catalysts with a series of dopants for the supercritical water gasification of empty palm fruit bunches to produce hydrogen. RSC Advances, 5, 36798-36808, 2015. https://doi.org/10.1039/C5RA03430B.

[21] M. Liang, W. Kang, K. Xie, Comparison of reduction behavior of Fe_2O_3, ZnO and $ZnFe_2O_4$ by TPR technique. Journal of Natural Gas Chemistry, 18, 110-113, 2009. https://doi.org/10.1016/S1003-9953(08)60073-0.

[22] Ö. Akarçay, S. F. Kurtoğlu, A. Uzun, Ammonia decomposition on a highly-dispersed carbon-embedded iron catalyst derived from Fe-BTC: Stable and high performance at relatively low temperatures. International Journal of Hydrogen Energy, 45, 28664-28681, 2020. https://doi.org/10.1016/j.ijhydene.2020.07.188.

[23] Z. P. Hu, C. C. Weng, C. Chen, Z. Y. Yuan, Two-dimensional mica nanosheets supported Fe nanoparticles for NH_3 decomposition to hydrogen. Molecular Catalysis, 448, 162-170, 2018. https://doi.org/10.1016/j.mcat.2018.01.038.

[24] W. Arabczyk, J. Zamlynny, Study of the ammonia decomposition over iron catalysts. Catalysis Letters, 60, 167-171, 1999. https://doi.org/10.1023/A:1019007024041.

[25] J. Zhang, M. Comotti, F. Schüth, R. Schlögl, D. S. Su, Commercial Fe- or Co-containing carbon nanotubes as catalysts for NH_3 decomposition. Chemical Communications, 19, 1916-1918, 2007. https://doi.org/10.1039/B700969K.

[26] T.V. Choudhary, C. Sivadinarayana, D. W. Goodman, Catalytic ammonia decomposition: CO_x-free hydrogen production for fuel cell applications. Catalysis Letters, 72, 197-201, 2001. https://doi.org/10.1023/A:1009023825549.